

Processing, Characterization, and Dielectric Studies on $K(\text{Ta}_{1-x}\text{Nb}_x)\text{O}_3$ for Use at Cryogenic Temperatures

Cristopher B. DiAntonio* and Stephen M. Pilgrim*

Laboratory of Electronic Ceramics, New York State College of Ceramics at Alfred University, Alfred, New York 14802

Development of the next generation space telescope, to supplement the Hubble Space Telescope, has heightened the need for cryogenic actuators. High performance electromechanical materials are needed for use from 10 to 77 K. The use of piezoelectric materials to satisfy this need involves major property trade-offs; consequently, alternative materials are of interest—the electrostrictive ceramics. The electrostrictors operate above their “Curie” (transition) temperature, and have electromechanical properties that can be superior to conventional piezoelectric materials. Because work on the electrostrictive materials is limited, the $K(\text{Ta,Nb})\text{O}_3$ solid solution system has been chosen as a viable material for use at cryogenic temperatures. These solid solutions have predicted transition temperatures in the range of 4 to 150 K. Two separate KTaO_3 powders were synthesized with 10 and 17.5 mol% Nb_2O_5 doping levels. The powders were synthesized via a conventional mixed oxide route and materials were fabricated using a tape cast and laminating technique. Powders and samples were characterized using laser scattering, scanning electron microscopy, and surface area analysis to determine particle size distribution and morphology, powder X-ray diffractometry for phase composition, and dielectric response as a function of frequency and temperature. Tape casting and lamination produced final samples that were fabricated to ~88% of theoretical density. Dielectric measurements resulted in Curie temperatures of 248 and 123 K, and weak-field permittivity values of ~2700 and 4000 for 17.5 and 10 mol% additions of Nb_2O_5 to KTaO_3 .

I. Introduction

RECENTLY, a need has developed for actuator and transducer systems for applications that operate at cryogenic temperatures. Examples of these applications include flow controllers for liquid fuels, micropositioners for high-temperature superconductors, precision positioning devices, active dampers for spacecraft, and transducers for ultrasonic monitoring of cryogenic liquids or structures. One group of materials that may be able to address this need is electrostrictive ceramics. These materials commonly operate above their transition temperature and have superior electromechanical properties. The KTaO_3 system seems to show potential as an electrostrictive ceramic, and will also be able to operate at cryogenic temperatures.

Matthias¹ reputed the ferroelectric properties of the compound KTaO_3 in 1949. The symmetry of the room temperature

phase is cubic and the lattice parameter is almost identical to that of KNbO_3 in its centrosymmetric phase, >700 K. Despite its similarity, the Curie temperature of KTaO_3 is believed to be ~13 K, one of the two lowest ferroelectric transition temperatures known to date (the other is that of lithium thallium tartrate monohydrate, $\text{LiTlC}_4\text{H}_4\text{O}_6\cdot\text{H}_2\text{O}$, 10 K). The temperature dependence of the dielectric constant has been measured down to 1.3 K by Hulm *et al.*² The results show that the dielectric constant obeys the Curie–Weiss law only down to 52 K, below which it still increases, but less rapidly than required by that law. A flat maximum is reached at the Curie point, below which the curve levels off in a smooth fashion. To date, no conclusive information is available about the symmetry of the polar phase. The deviation from the Curie–Weiss law at low temperatures is a phenomenon characteristic of ferroelectrics with very low Curie points.² Barrett³ showed that quantum effects play an important role in these low temperature regions, and that these effects can explain the deviation from the Curie–Weiss law observed experimentally.

The $K(\text{Ta}_{1-x}\text{Nb}_x)\text{O}_3$ (KTN) system is a ferroelectric material for $x \geq 0.05$, and exhibits the same three ferroelectric phases as BaTiO_3 and KNbO_3 (tetragonal–orthorhombic–rhombohedral). It has a high pyroelectric coefficient of $\sim 4 \times 10^{-6} \text{ } ^\circ\text{C}\cdot(\text{m}^2\cdot\text{K})^{-1}$. Its Curie temperature can vary with the composition from 13 K for KTaO_3 , to 700 K for KNbO_3 , and it is stable in air. The phase diagram and variation in Curie temperature for this solid solution can be seen in Fig. 1. The system of solid solutions $K(\text{Ta,Nb})\text{O}_3$ was first investigated by Reisman *et al.*^{3,4} with thermal and XRD measurements. Triebwasser⁵ conducted a detailed study of this system more recently with particular attention to its dielectric properties. The measurements were made on single crystals of solid solutions with different compositions. Single-crystal KTN and hot-pressed polycrystalline KTN, prepared from the conventional mixed oxide method, have been studied by other investigators.^{6–9} The results show that the Curie temperature varies almost linearly between the two end-members of the system with a cubic–tetragonal transition in the region of room temperature when $x \approx 0.37$ (see Fig. 1). The predicted transition temperatures for the synthesized compositions are 298 and 173 K for Nb_2O_5 dopant levels of 17.5 and 10 mol%, respectively. These predicted values have been determined from Fig. 1.

II. Experimental Procedure

Potassium carbonate (K_2CO_3 , 99% purity, standard grade, EM Science, Gibbstown, NJ), tantalum oxide (Ta_2O_5 , 99% purity, ceramic grade, H. C. Stark, Inc., New York), and niobium oxide (Nb_2O_5 , 99% purity, ceramic grade, H. C. Stark, Inc.), were used as raw materials. Thermogravimetric (TGA) and differential thermal analysis (DTA) were performed before batching to determine the amount of volatiles in each of the raw materials, and to quantify the hygroscopic nature of the K_2CO_3 .

W. Huebner—contributing editor

Manuscript No. 188508. Received June 5, 2000; approved October 16, 2000.
Presented at the 100th Annual Meeting of the American Ceramic Society, Cincinnati, OH, 1998.
*Member, American Ceramic Society.

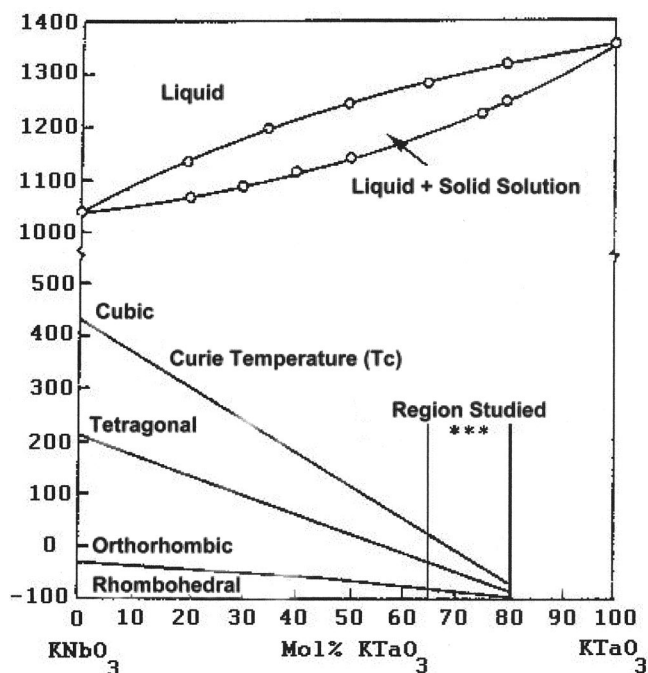
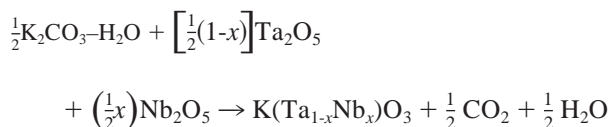


Fig. 1. Phase diagram of the KNbO_3 - KTaO_3 system.^{5,6}

For clarity purposes, the base powder is considered KTaO_3 and the dopant is Nb_2O_5 . This results in a formulation equation of the type[†]



Two separate compositions were prepared, one with 10 mol% Nb_2O_5 , and the other with 17.5 mol% Nb_2O_5 . For both compositions, the K_2CO_3 , Nb_2O_5 , and Ta_2O_5 were dry- and wet-ball-

[†]The evolved CO_2 and absorbed H_2O must be accounted for.

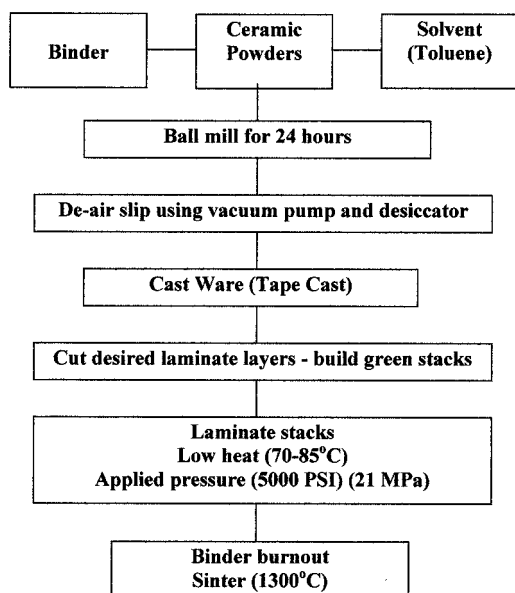


Fig. 2. Flowchart showing the general steps for fabricating samples from laminated tape-cast layers.

Table I. Heat Treatment Schedule used for Binder Burnout and Sintering of the KTN Laminated Stacks

Temperature ramp (°C/h)	Dwell temperature (°C)	Dwell time (h)
20	350	4
30	450	4
40	600	2
200	1300	2

milled using stabilized zirconia. The powders were first dry-milled to break down agglomerates and promote mixing. After dry-milling for 2 h, ethanol was added and the powders were wet-milled for 24 h. Ethanol was used because the K_2CO_3 not only absorbs water, but also is soluble in it. It is assumed that no dissolution of K_2CO_3 into the ethanol occurred. The suspension was then stir-dried. The powder was calcined in a sealed alumina crucible (calciner furnace controlled by a control unit, Eurotherm Corp., Reston, VA) to 850°C and held there for 4 h. After calcination, the powder was dry-ball-milled for 4 h to reduce the particle size and pulverize the larger agglomerates that formed during calcining. The calcination/milling procedure was then repeated to assure the reaction had completed.

Final test samples were fabricated using a tape cast and laminating technique. Figure 2 is a flow chart that shows the general steps taken to prepare a sample from laminating tape layers produced by tape casting. The slurry prepared for casting was composed of 65% KTN powder, 29% binder (No. B73305 vinyl binder system, Ferro Corp., Cleveland, OH) and 6% toluene (solvent) by weight. This particular binder is formulated with all necessary solvents, plasticizers, surfactants, and release additives. The slurry was then mixed for 24 h using zirconia milling media. It is important not to ball-mix for longer periods than 24 h because of evaporation of organic substances and mechanical degradation of the vinyl binder. The degradation of the binder can occur because of the milling action of the media, which is added only to promote mixing and homogeneity. The slurry is de-aired, using a vacuum pump and desiccator, and cast, using a doctor blade casting unit. The tape was dried for 45 min inside a vented chamber. The tape was cut, stacked and laminated using a laboratory press (Carver, Inc., Wabash, IN) that is equipped with a heating system (Model CN 800, Omega Engineering, Inc., Stamford, CT). This heating system controls the temperature of the press plates, both above and below the die. The stacks were laminated at 75°C , 5000 psi (20.7 MPa), and held for 10 min.

The final samples were sintered to 1300°C for 2 h (alumina tube furnace, Lemont Scientific, State College, PA, controlled by a Eurotherm control unit). They were fired in a sealed alumina crucible and the atmosphere was maintained by packing the

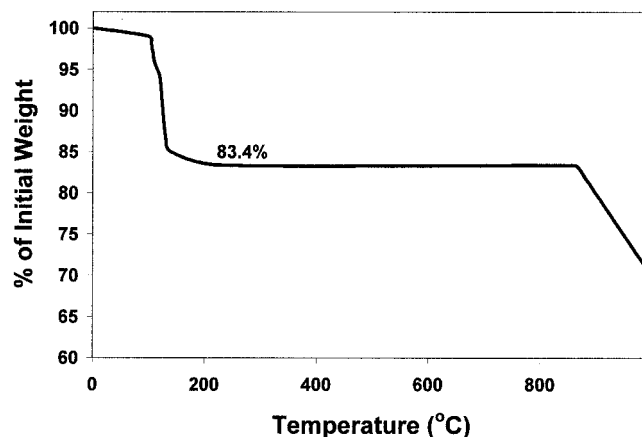


Fig. 3. TGA profile for K_2CO_3 , tested at $10^\circ\text{C}/\text{min}$ up to 1000°C .

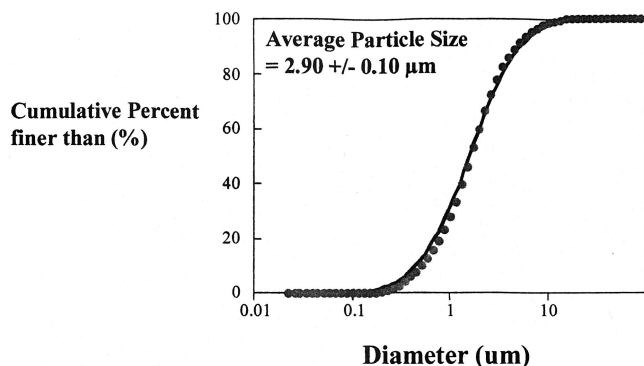


Fig. 4. Laser-scattering particle-size distribution analysis.

samples in a sacrificial powder of the same composition. The sintering schedule for the laminates has several steps because of the high percentage of organics that need to be burned out. The heat treatment schedule shown in Table I was used for binder burnout and sintering of the KTN laminated stacks.

The sintered samples were polished using 320 and 600 grit SiC polishing paper. Polished sample surfaces were sputtered with a layer of 60% gold–40% palladium and then electroded using a silver, fire-on, conductor composition (silver conductor composition No. 7095, Dupont, Wilmington, DE). The silver paste was fired on at 550°C for 15 min.

To fully characterize the powders, a number of powder characterization techniques were used. TGA was used to quantify the amount of volatiles in the raw materials, particularly K_2CO_3 . The particle size distribution and morphology were measured using a combination of SEM, laser scattering analyzer, and surface area analysis (BET). Phase purity and phase development of the final powders was examined using powder XRD. The density of the powder was determined using a helium pycnometer, and the specific surface area was measured using BET analysis.

III. Results and Discussion

(1) TGA of Raw Materials

TGA was performed on all raw materials used for batching KTN. The tantalum and niobium oxide showed no indication of

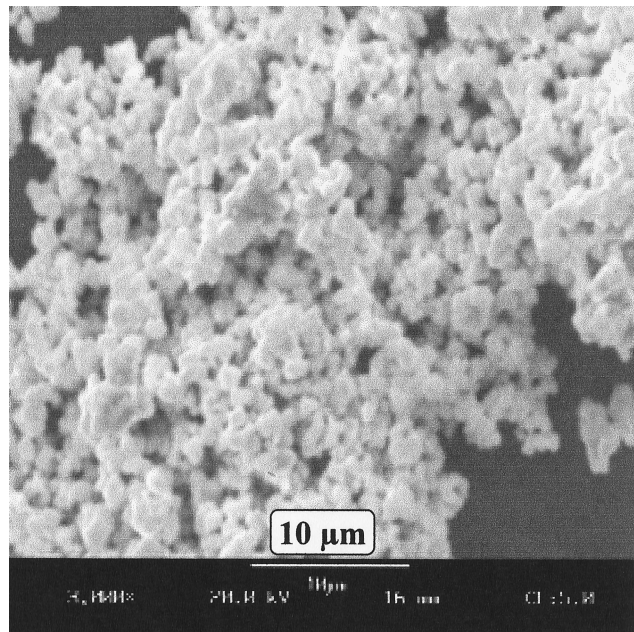


Fig. 5. SEM image of final KTN ($x = 0.20$) powder at 4000 \times magnification.

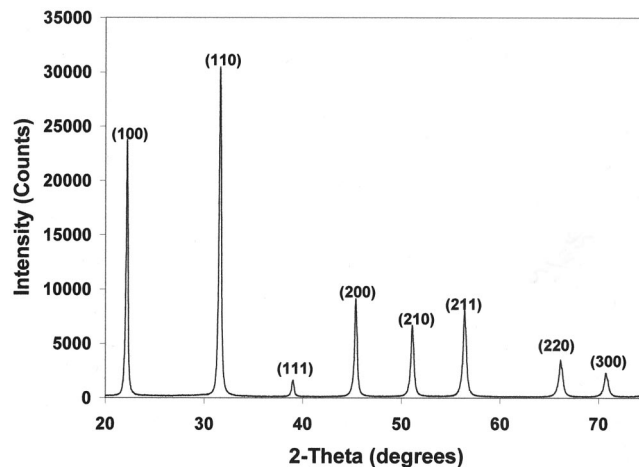


Fig. 6. XRD pattern of KTN¹¹ ($x = 0.20$).

any decomposition products or volatiles. The TGA for potassium carbonate is shown in Fig. 3. The analysis was performed using a heating rate of 10°C/min to 1000°C. The initial weight loss at 100°C is caused by the volatilization of absorbed water. At 860°C, the carbonate decomposes and carbon dioxide volatilizes, leaving a pure form of potassium oxide (K_2O). The TGA results show that K_2CO_3 contains ~16.6% by weight of absorbed H_2O . This was taken into consideration in the batch formulations.

(2) Powder Properties

Powders with Nb_2O_5 dopant levels of 0.17 [$K(Ta_{0.65}Nb_{0.35})O_3$] and 0.10 [$K(Ta_{0.80}Nb_{0.20})O_3$] were synthesized using conventional mixed oxide techniques. The particle size distribution (Model LA-920, Laser Scattering Particle Size Distribution Analyzer, Horiba Instruments, Inc., Irvine, CA) and a SEM image (Model 1810, Amray, Inc., Bedford, MA) of the calcined powder can be seen in Figs. 4 and 5. From the SEM image and particle size distribution results, the average particle size was determined as $2.90 \pm 0.10 \mu\text{m}$, assuming spherical particles. This value was consistent for both powders ($x = 0.35$ and $x = 0.20$) prepared in this system. The image also shows the spherical-like morphology of the particles. BET analysis measured the specific surface area (Model Gemini III 2375 Surface Area Analyzer, Micromeritics, Norcross, GA) of the calcined powders at a value of $2.5 \pm 0.35 \text{ m}^2/\text{g}$.

(3) Phase Formation

Final powders were examined for phase formation and purity using powder XRD techniques (Model D5000, Siemens, Karlsruhe, Germany; JADETM pattern processing software, Materials Data, Inc., Livermore, CA). Figure 6 shows a typical XRD pattern of the $x = 0.20$ KTN composition (all patterns were taken over a 2θ range of 20° to 70° and a step size of 0.02° at a count time of 5 s). The major phase in both compositions was the cubic perovskite $KTaO_3$, $Pm\bar{3}m$. The KTN, $x = 0.20$ and $x = 0.35$, patterns are nearly identical to each other. The only difference, as seen in X-ray analysis, is a small shift in the 2θ values and a slight broadening at the base of the peaks. These changes are caused by the small variation in unit cell size from the further substitution of niobium for tantalum at $x = 0.35$. The pattern was compared with both end compositions $KTaO_3$ and $KNbO_3$ (Refs. 11 and 12, respectively) because a reliable solid solution pattern doesn't exist in the powder diffraction file database. $KNbO_3$, at room temperature, has an orthorhombic crystal structure ($Cm2m(38)$). No unidentified peaks were present and the pattern indexes as cubic with the (hkl) values, as noted in Fig. 6.

The XRD analysis confirmed phase formation with no indication of contamination. The pattern matched that of the cubic perovskite $KTaO_3$ (Ref. 11) and no $KNbO_3$ peaks were apparent in

Table II. Physical Properties of the Laminated Pellets of KTN ($x = 0.35$ and $x = 0.20$)[†]

Applied pressure (psi)	Apparent porosity (%)	Bulk density (g/cm ³)		Percent of theoretical density (%)	
		$x = 0.35$	$x = 0.20$	$x = 0.35$	$x = 0.20$
2500 (17 MPa)	12 ± 1	5.0 ± 0.30	5.3 ± 0.20	80.9 ± 3	81.0 ± 5
3500 (24 MPa)	6.7 ± 4	5.3 ± 0.25	5.5 ± 0.30	85.8 ± 3	84.0 ± 3
4000 (28 MPa)	5.3 ± 2	5.5 ± 0.35	5.6 ± 0.25	89.0 ± 1	85.6 ± 2
5000 (34 MPa)	5.0 ± 3	5.7 ± 0.40	5.8 ± 0.20	92.2 ± 1	88.7 ± 1

[†] ρ_T (theoretical density) calculated as 6.18 g/cm³ for $x = 0.35$ and 6.54 g/cm³ for $x = 0.20$ (XRD).

the pattern, indicating the formation of a solid solution of K(Ta,Nb)O₃. The only indication of the added Nb₂O₅ dopant was a slight shift of the diffraction peaks at the 17.5 mol% niobium oxide composition caused by the change in lattice spacings with increasing Nb⁵⁺ substitution for Ta⁵⁺ in the unit cell. The Nb⁵⁺ and Ta⁵⁺ occupy the same site in the perovskite structure, and the difference in their ionic radius is only ~0.02 Å, therefore, the cubic KTaO₃ X-ray pattern appears to dominate at dopant levels of 0.20 and smaller.

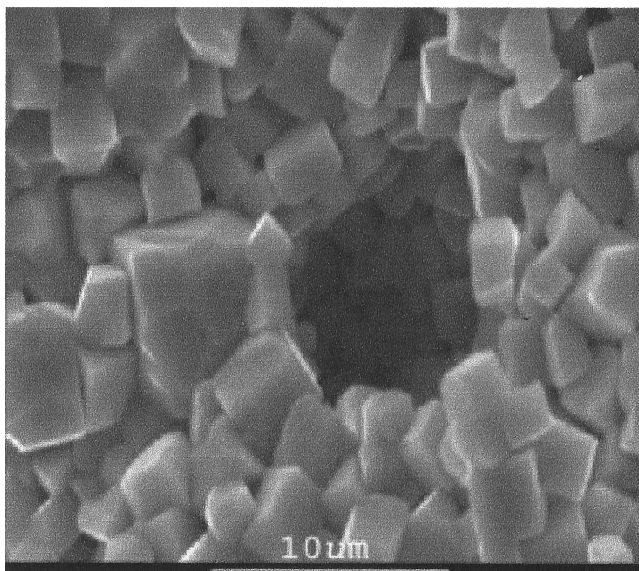
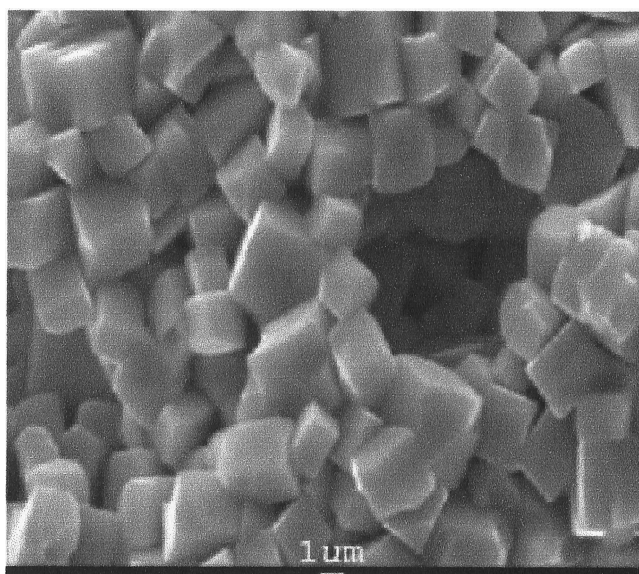


Fig. 7. SEM images of fractured surfaces of KTN ($x = 0.20$).

(4) Sintering Behavior

The percent of theoretical density, apparent porosity, and bulk density, as a function of pressing pressure, was measured for the KTN samples following a previously outlined procedure.¹³ Several laminating pressures were tested to find the ideal conditions for the sample fabrication, and those results are listed in Table II for both the $x = 0.35$ and $x = 0.20$ sintered samples. Density values of ~88% of the theoretical density were the best obtained because of the difficulty in sample preparation. The KTN solid solution appears to sinter at high temperatures (1300°C) and maximum densification. At higher temperatures, density values remained the same and eventually led to melting of the samples. The optimal laminating condition for these samples is an applied pressure of 5000 psi at 75°C. These conditions provided consistent results and well-fabricated samples for testing. The average volume shrinkage, from green to fired state, was ~25 vol% after sintering to 1300°C.

(5) Microstructure

The microstructure of the final samples was examined using SEM. A fractured surface of a pellet of KTN $x = 0.20$ is shown in Fig. 7. Both KTN compositions possessed the same microstructural characteristics. Visual inspection of these images indicates that grain sizes are on the order of 3–5 μm and undergo intergranular fracture. Also evident in these images are the large volumes of porosity contained in these samples.

(6) Dielectric Measurements

Dielectric measurements were performed as a function of frequency and temperature (Model 4284A, precision LCR meter, Model 3488A, automatic switch scanner, Hewlett-Packard Co., Rockaway, NJ, and a test chamber, Delta Design, San Diego, CA, controlled by a computer running LabView software, National Instruments, Woburn, MA). The test chamber was capable of operating in the temperature range of 90 to 475 K (using liquid nitrogen to cool), thus allowing measurements over a broad temperature range. True four-point contacts were made at the sample (as shown in Fig. 8), rather than at the back end of the probe. The chamber was heated to 445 K and held for 30 min to allow moisture to volatilize and fully de-age the samples. Samples that are not properly de-aged will show lower permittivity values,

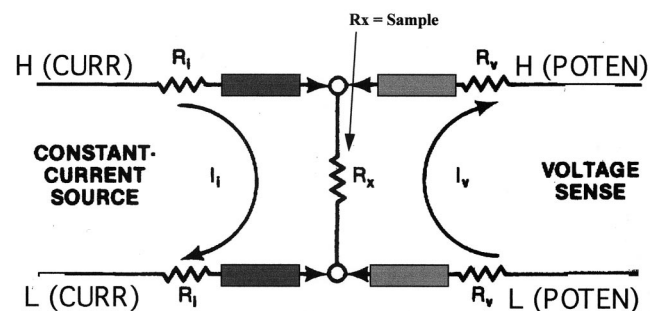


Fig. 8. Four-terminal measurements largely eliminate the effects of lead resistance by separating the current-sourcing and voltage-sensing functions.

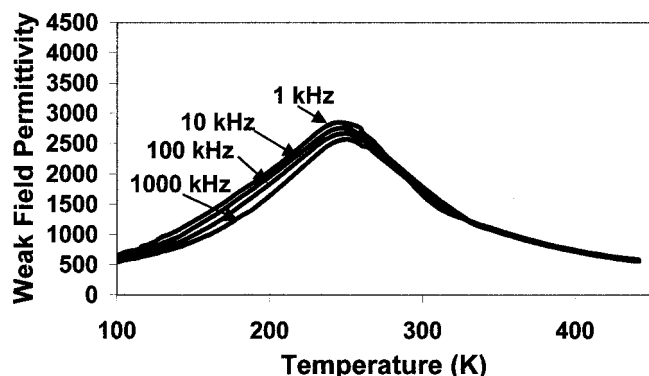


Fig. 9. Weak-field permittivity measurements of KTN ($x = 0.35$) as a function of frequency and temperature.

shifted transition temperatures, and relaxation frequencies. Data were then collected from 445 to 90 K with a -1 K/min cooling rate and liquid nitrogen purging the oven.

The average weak-field permittivity and dielectric loss as a function of temperature and frequency for KTN, $x = 0.35$ and $x = 0.20$, is shown in Figs. 9–12. The measurements were taken over a temperature range of 445 to 90 K for frequencies of 1, 10, 100, and 1000 kHz at 1 Vrms applied voltage. The permittivity values were collected on the cooling portion of the temperature cycle. The average transition temperature (T_{max}) and average permittivity at that T_{max} as a function of frequency for the $x = 0.35$ and $x = 0.20$ samples, are listed in Tables III and IV. Figure 13 shows a comparison of the weak-field permittivity for KTN ($x = 0.20$ and $x = 0.35$) as a function of temperature at a frequency of 1 kHz. It is easy to see the difference in the magnitude and overall diffuseness between the two samples.

The diffuseness of the transition for $x = 0.35$ and $x = 0.20$ has been calculated using the Gaussian distribution relation:¹⁰

$$E_{rmax} = E_r \exp[(T_i - T_0)^2 / 2\delta_g^2]$$

where E_{rmax} is the maximum relative dielectric constant, E_r the relative dielectric constant, and δ_g the Gaussian diffuseness. The calculated values are included in Tables III and IV. A method of limiting the temperature range to that corresponding to two-thirds of the maximum relative dielectric constant was used to calculate the diffuseness.¹⁰ One of the possible reasons for diffuse phase transitions in ferroelectric solid solutions is that fluctuations in composition occur. The diffuseness values characterize the breadth of the transition peak and allow for another way of comparing the homogeneity of the compositions to each other. The diffuseness value for the $x = 0.35$ is higher than those for the $x = 0.20$ composition. The higher values may indicate that more fluctuations in the composition are present for a larger Nb_2O_5 doping level.

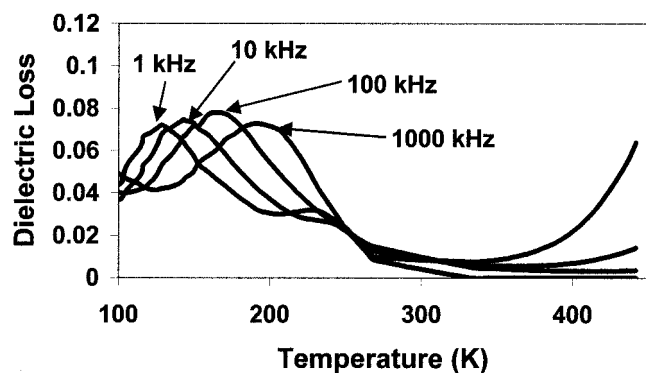


Fig. 10. Dielectric loss for KTN ($x = 0.35$) as a function of temperature and frequency.

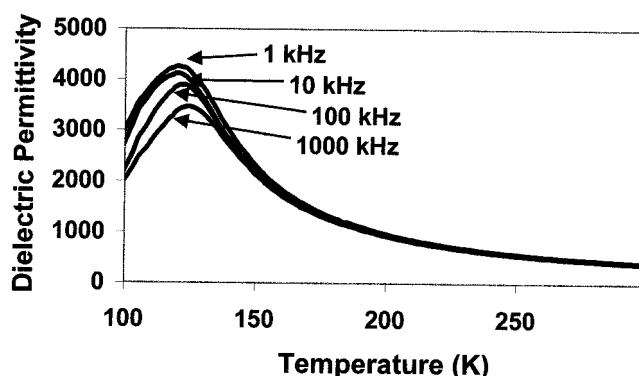


Fig. 11. Weak-field permittivity measurements of KTN ($x = 0.20$) as a function of frequency and temperature.

IV. Conclusions

These results provide a clearer view of the powder properties, microstructural characterization, and dielectric response of two separate solid solutions in the KTN system. Although both compositions show similar physical properties, their dielectric properties are significantly different. TGA allowed quantification of volatiles in the potassium carbonate where 16.6% by weight of the material is adsorbed H_2O . The tape casting and laminating technique produced samples with densities greater than 88% of theoretical.

The dielectric results show broad transition curves and a frequency dispersion that is dependent on the temperature of the measured variables. This is characteristic of relaxor ferroelectric behavior. The temperatures of maximum dielectric constant, T_{max} , also exhibit relaxor-type frequency dependence. Relaxor ferroelectrics undergo a diffuse phase transition between the low-temperature ferroelectric phase and the high-temperature paraelectric phase over a wide temperature range. This behavior is apparent for the KTN material. The decrease in the Nb_2O_5 doping level, from 17.5 to 10 mol%, resulted in a decrease of the T_{max} from 250 to 120 K. These values differed significantly from those predicted by Fig. 1. Also evident was an increase in the average weak-field permittivity for all frequencies tested. The difference of maximum permittivity values and transition temperatures between $KTa_{0.65}Nb_{0.35}O_3$ and $KTa_{0.80}Nb_{0.20}O_3$ suggests that the random occupation of the same site with different cations result in local variations of composition and the local transition temperature. However, further work is needed at lower dopant levels and lower temperatures to confirm the dielectric nature of KTN for cryogenic use.

The KTN system shows potential as a base material for low-temperature electroactive dielectrics. The system exhibits typical

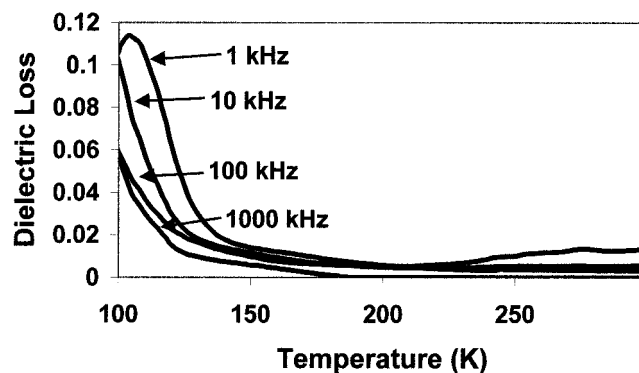


Fig. 12. Dielectric loss for KTN ($x = 0.20$) as a function of temperature and frequency.

Table III. Average Curie Temperature (T_{\max}), Average Permittivity, and Diffuseness as a Function of Frequency for KTN ($x = 0.35$)

Frequency (kHz)	Average T_c (max)	Average permittivity	Diffuseness (K)
1	242 ± 3.0 K	2850 ± 19.0	55.6 ± 1.5
10	246 ± 1.8 K	2750 ± 15.0	50.2 ± 2.0
100	248 ± 3.2 K	2660 ± 15.0	51.2 ± 3.5
1000	250 ± 2.5 K	2570 ± 20.0	52.2 ± 4.0

Table IV. Average Curie Temperature (T_{\max}), Average Permittivity, and Diffuseness as a Function of Frequency for ($x = 0.20$)

Frequency (kHz)	Average T_c (max)	Average permittivity	Diffuseness (K)
1	121 ± 1.0 K	4260 ± 2.5	23.3 ± 2.0
10	123 ± 2.8 K	4120 ± 3.0	21.5 ± 1.5
100	124 ± 2.2 K	3900 ± 6.0	22.3 ± 3.0
1000	126 ± 3.5 K	3470 ± 8.5	24.3 ± 4.5

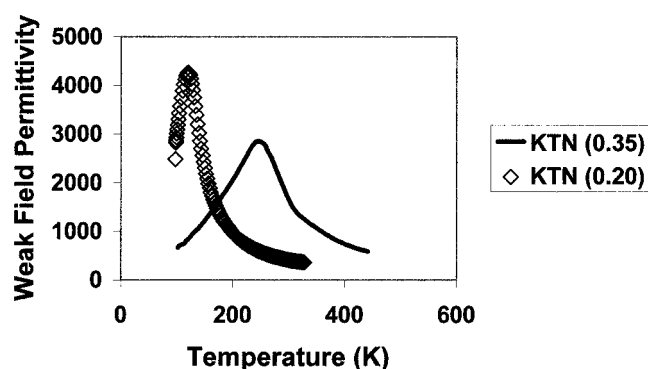


Fig. 13. Comparison of the weak-field permittivity for KTN ($x = 0.20$) and KTN ($x = 0.35$) as a function of temperature for a frequency of 1 kHz.

relaxer ferroelectric behavior with a strong dependence on temperature and frequency. Extensive characterization is essential in determining and reporting the electroactive responses of a device. Often, powder and final sample features are excluded or not given the level of importance they deserve. Past and present research indicates that variations in average grain size, percent porosity, phase purity, etc., can have profound effects on the dielectric properties of a device. The potential they have to vary properties of the material and device is enormous, making it essential to examine the characteristics of a powder system. However, to fully quantify the potential of the KTN system, the electromechanical response of these devices needs to be investigated. This will be a better indicator of the compositions viability in the area of electroactive devices and is the goal of future work.

References

- ¹B. T. Matthias, "New Ferroelectric Crystals," *Phys. Rev.*, **75** [11] 1771 (1949).
- ²J. K. Hulm, B. T. Matthias, and E. A. Long, "A Ferromagnetic Curie Point in KTaO_3 at Very Low Temperatures," *Phys. Rev.*, **79** [5] 885 (1950).
- ³J. H. Barrett, "Dielectric Constant in Perovskite Type Crystals," *Phys. Rev.*, **86** [1] 118 (1952).
- ⁴A. Reisman and E. Banks, "Reactions of the Group VB Pentoxides. VIII. Thermal, Density and X-Ray, Studies of the Systems $\text{KNbO}_3\text{-NaNbO}_3$ and $\text{KTaO}_3\text{-KNbO}_3$," *J. Am. Chem. Soc.*, **80** [8] 1877 (1958).
- ⁵S. Triebwasser, "Study of Ferroelectric Transitions of Solid-Solution Single Crystals of $\text{KNbO}_3\text{-KTaO}_3$," *Phys. Rev.*, **114** [1] 63 (1959).
- ⁶A. Reisman, S. Triebwasser, and F. Holtzberger, "Phase Diagram of the System $\text{KNbO}_3\text{-KTaO}_3$ by the Methods of Differential Thermal and Resistance Analysis," *J. Am. Chem. Soc.*, **77** [16] 4228 (1955).
- ⁷J. D. Siegwarth and J. C. Holste, "Polarization and Dielectric Constant of Potassium Tantalate," *J. Appl. Phys.*, **47** [11] 4791-93 (1976).
- ⁸P. E. Debely, P. Gunter, and H. Arend, "Preparation and Electro-optic Properties of Hot-Pressed Potassium Niobate-Tantalate Ceramic," *Am. Ceram. Soc. Bull.*, **58** [6] 606-609 (1979).
- ⁹A. L. Gentile and F. H. Andres, "A Constant Temperature Method for the Growth of KTN Single Crystals," *Mater. Res. Bull.*, **2** [4] 353 (1967).
- ¹⁰S. M. Pilgrim, S. R. Sutherland, and A. E. Winzer, "Diffuseness as a Useful Parameter for Relaxor Ceramics," *J. Am. Ceram. Soc.*, **73** [10] 3122-25 (1990).
- ¹¹Powder Diffraction File Card No. 38-1470. International Centre for Diffraction Data, Newton Square, PA, 1989.
- ¹²Powder Diffraction File, Card No. 32-0822; see Ref. 11, 1983.
- ¹³"Standard Test Methods for Liquid Absorption, Apparent Porosity, Apparent Specific Density, and Bulk Density by Vacuum Pressure," ASTM Designation C 830-88, American Society for Testing and Materials, West Conshohocken, PA, 1988. □